Korean J. Chem. Eng., 33(7), 2050-2062 (2016)
DOI: 10.1007/s11814-016-0039-0

pISSN: 0256-1115
eISSN: 1975-7220

Mechanism of methane hydrate formation in the presence of hollow silica

Hari Prakash Veluswamy*, Pinnelli Seetha Rama Prasad, and Praveen Linga*,†**

*Department of Chemical and Biomolecular Engineering, National University of Singapore, Singapore 117 585, Singapore
**Gas Hydrate Division, National Geophysical Research Institute, Council for Scientific and Industrial Research, Uppal Road, Hyderabad 500 007, India

(*Received 5 October 2015 • accepted 4 February 2016*)

Abstract−Methane hydrates are studied extensively as a prospective medium for storing and transporting natural gas due to their inherent advantages, including high volumetric energy storage density, being environmentally benign and extremely safe method compared to conventional compression and liquefaction methods. Enhanced formation kinetics of methane hydrates has been reported in hollow silica due to the increased gas/liquid contact surface area available for efficient conversion of water to hydrates. This work elucidates the mechanism of methane hydrate formation in light weight hollow silica. Hollow silica-to-water ratio was varied and its effect on the methane hydrate formation/dissociation morphology was observed. There exists a critical hollow silica-to-water ratio (1 : 6) beyond which the hydrates preferentially crystallize on the top of the bed by drawing water from the interstitial pores, whereas below this ratio the hydrate formation occurs within the bed between inter-particular spaces of hollow silica. Due to the very low bulk density, a small fraction of hollow silica was observed to be displaced from the bed during the hydrate formation above the critical hollow silica to water ratio.

Keywords: Gas Hydrates, Methane Hydrate, Morphology, Hollow Silica, Gas Storage

INTRODUCTION

Methane is the major constituent of natural gas that serves as a greener fuel source resulting in lesser carbon dioxide emission than fossil fuels and other hydrocarbon-based fuels. Conventional methods for storage and transport of natural gas include compression and liquefaction. Compressed natural gas (CNG) storage necessitates the requirement of thick walled and heavy cylindrical tanks capable of withstanding higher degree of compression to result in approximately one-third volumetric energy storage density of gasoline. Liquefied natural gas (LNG) is comparatively efficient with its volumetric energy storage density approximately two-thirds of gasoline, yet is quite expensive requiring extensive pressurization and cooling below the critical temperature of methane, 190.6 K [1,2] accompanied with substantial boil-off losses due to cryogenic storage conditions [3,4]. This necessitates the requirement of other modes of storage and transport of natural gas. Storing and transporting natural gas in the form of hydrates is promising and viable due to their significant advantages like high gravimetric/volumetric energy storage density with the potential to store about 170 m^3 of natural gas in just 1 m^3 of hydrate at STP [5], being environmentally benign (involves usage of only water as a solvent), easy to recover the stored gas using any waste heat stream or sea water as circulating heat exchange fluid and offer a very safe mode (as hydrates are non-explosive) of energy storage compared to conventional energy storage methods. Also, the recoverability of methane from stored hydrates is easy and can be achieved by thermal stimulation, de-pressurization or a combination of these two approaches [6,7]. Apart from methane (natural gas), hydrates are also actively researched for their considerable advantages in carbon dioxide capture [8], hydrogen storage [9,10] and desalination [11] applications.

Natural gas hydrates (NGH) are crystalline, non-stoichiometric, inclusive compounds that enclose guest gas molecules in the cages formed by host water molecules [12-14]. Methane gas, a dominant component in natural gas forms sI type hydrate structure with unit cell comprised of two small dodecahedron (5^{12}) cages and six large tetrakaidecahedron ($5^{12}6^2$) cages formed by 46 water molecules [14]. Natural gas hydrate deposits are found to occur naturally in marine sediments along the continental margins and in the permafrost locations along the polar regions. Huge amount of methane is present in NGH resources that are evenly distributed across the world [15-17]. Natural gas storage and transport in the form of hydrate pellets has been made feasible and there exist pilot scale plants in Japan and South Korea producing hydrate pellets [18-20]. 'Self-preservation effect' observed during the dissociation of methane hydrates below the freezing point of water (<273.2 K) aids in efficient storage and transport of natural gas at temperature conditions in the range of 242-271 K [21-23]. It has been identified that a major bottleneck on the application of the clathrate hydrate technology for energy storage and transport is the kinetics (how fast and how much of gas capacity storage is achievable in these materials) [24,25]. To this end, many researchers focus on enhancing the kinetics of methane hydrate formation either by the usage of kinetic promoters like surfactants [26-30] or amino acids [25], or by developing innovative reactor configurations to contact the gas and liquid with or without promoters [31-34]. Recently, few

†To whom correspondence should be addressed.
E-mail: Praveen.Linga@nus.edu.sg, chepl@nus.edu.sg
Copyright by The Korean Institute of Chemical Engineers.

studies have presented enhanced kinetics with a use of porous medium for methane hydrate formation. Different materials like silica gel, activated carbon, carbon nanotubes, dry water, dry gel, nanosilica and aluminium foam have been used as fixed bed support to study the methane hydrate formation kinetics [35-43]. Dry water is a mixture prepared using water, hydrophobic silica and air at very high mixing speeds of about 19,000 rpm resulting in free flowing powder. However, the reusability of such a mixture for successive hydrate formation cycles has been a challenge and has been reported to reduce the gas uptake performance and the storage capacity of methane. To overcome this problem, dry gel system was proposed which had an additional gelling agent, gellan gum added to the dry water that yielded better recyclability of the material for successive hydrate formation cycles. However, handling/maintenance issues along with the need for very high speed mixing (which is costly) hinder the application of these materials in forming methane hydrates on a larger scale so far. Also, while the kinetics of hydrate formation is enhanced with the presence of porous materials, its impact on the overall process chain of natural gas hydrate storage and transport is not well understood. For instance, the impact of the volumetric increase due the presence of porous material, the challenges in the hydrate pelletizing step and challenges encountered during the transport of hydrates in the presence of porous materials are yet to be explored/demonstrated. Though many of the above listed materials have been proven to enhance the methane hydrate formation kinetics, it has also been reported that hydrophobic silica particles and activated carbon inhibit the hydrate formation at water/oil interface [44,45].

Hollow silica has been proposed as an alternate material for being used as porous medium for enhancing the kinetics of methane hydrate formation [46-49]. Hollow silica structure consists of an inner void surrounded by a thin solid outer shell that has several advantageous properties, including extremely low bulk density, high porosity, high surface area etc. Although enhanced kinetics has been reported in the literature, the exact mechanism of hydrate growth in the presence of hollow silica and the reason for the kinetic rate enhancement is not known in the literature.

Hence, the objective of this work is to elucidate the mechanism of hydrate formation in hollow silica and to understand the reason for enhanced kinetics in the presence of hollow silica. The current study focuses on the hydrate growth mechanism occurring in the bed of hollow silica by coupling morphology and kinetic data measurements.

EXPERIMENTAL SECTION

1. Materials

Hollow silica powder of 99% purity with mean diameter of 30-70 μm having bulk density of <0.1 g/cm^3 was used in all experiments and the same material was used in earlier studies of CSIR-NGRI group [46,48]. 99.9% methane in compressed cylinder procured from SOXAL and distilled water made using Elga micromeg deionizaton apparatus were used for conduction of experiments.

2. Apparatus

The experimental setup used was the same as detailed by Veluswamy et al. [50]. 28 L Polyscience 9612 model circulator was used to circulate and maintain the temperature of the crystallizer contents. Pressure in the crystallizer was measured digitally using a Rosemount 3051 pressure transmitter with a maximum uncertainty of 0.1% in the pressure range of 0 to 20 MPa and a pressure gauge supplied by WIKA provided analogue measurement of the crystallizer pressure. Copper-constantan T type thermocouple supplied by Omega having an uncertainty of 0.1 K was used for recording the crystallizer temperature. Data acquisition (DAQ) system supplied by National Instruments, connected to a computer, was used to record the crystallizer temperature and pressure relayed from the thermocouple and pressure transmitter, respectively. Images of hollow silica bed during the experiment were captured using SMZ1000 Stereoscopic zoom microscope from Nikon coupled along with Nikon Digital Sight (DS-Fi1) Camera for every 20 seconds throughout the cycle of formation and dissociation experiments.

3. Experimental Procedure

0.5 g of hollow silica was used for all the experiments conducted; 4, 3 and 2 ml of water were considered for different experiments such that the ratios of silica to water by weight were 1 : 8, 1 : 6 and 1 : 4 respectively. These ratios by weight were considered as the hollow silica was reported to be saturated in the range of 1 : 4 to 1 : 6 ratio in the earlier study reported by Prasad [48]. 1 : 8 ratio (well above other two ratios) resulted in excess saturation and was investigated in detail in this study. Due to the light weight of hollow silica particles used, a thin layer of water was observed to be present beneath the hollow silica bed, signifying that the bed was completely saturated for 1 : 8 ratio of hollow silica to water. For other two ratios considered there was no observable water present at the bottom of the reactor. Similar observations were recorded when using such silica to water ratio in the study conducted by Prasad [48]. After the hollow silica bed preparation, top SS flange was mounted on the acrylic column and both the flanges were tightened making the crystallizer suitable for pressurization.

All experiments were conducted at a starting pressure of 8.0 MPa and constant temperature of 278.2 K to map the experimental conditions reported on this material in the literature [48]. Equilibrium pressure at 278.2 K was reported to be 4.3 MPa by Nakamura et al. [51]. Thus, a driving force of 3.7 MPa was provided for all hydrate formation experiments. After setting up the hollow silica bed in the transparent acrylic column as per the procedure detailed earlier, it was observed that the silica bed was approximately 2 cm in height. After cooling to the experimental temperature of 278.2 K, the crystallizer was pressurized to 8.0 MPa with methane gas after initial purging to about 1 MPa pressure in order to remove the initial air present inside the crystallizer. After pressurization, the height of the silica bed decreased to around 1 cm because of the extremely low bulk density of the hollow silica particles (<0.1 g/cm^3). Few wetted hollow silica particles are seen attached to the wall of the crystallizer due to the compression of bed during pressurization/depressurization. Wetted hollow silica particles also imply that the bed has been completely saturated with water. Fig. S1 in the supporting information shows images of the hollow silica bed before and after pressurization for hollow silica to water ratio of 1 : 8. It can be observed that there is approximately half the bed height reduction after achieving the experimental pressure in the crystallizer. Crystallizer was maintained at experimental conditions till

the hydrate formation takes place.

The pressure and temperature trace of a complete experimental cycle for a typical morphology experiment is presented in Fig. 1. Four distinct stages are observed during each of the experimental trials conducted (Fig. 1(e)). The first stage after setting the crystallizer with hollow silica is cooling the content of the crystallizer to experimental temperature. The crystallizer was purged and pressurized with methane gas to around 1 MPa to remove air present initially inside the crystallizer. The first step was the cooling step from room temperature, 298.2 K, to the experimental temperature

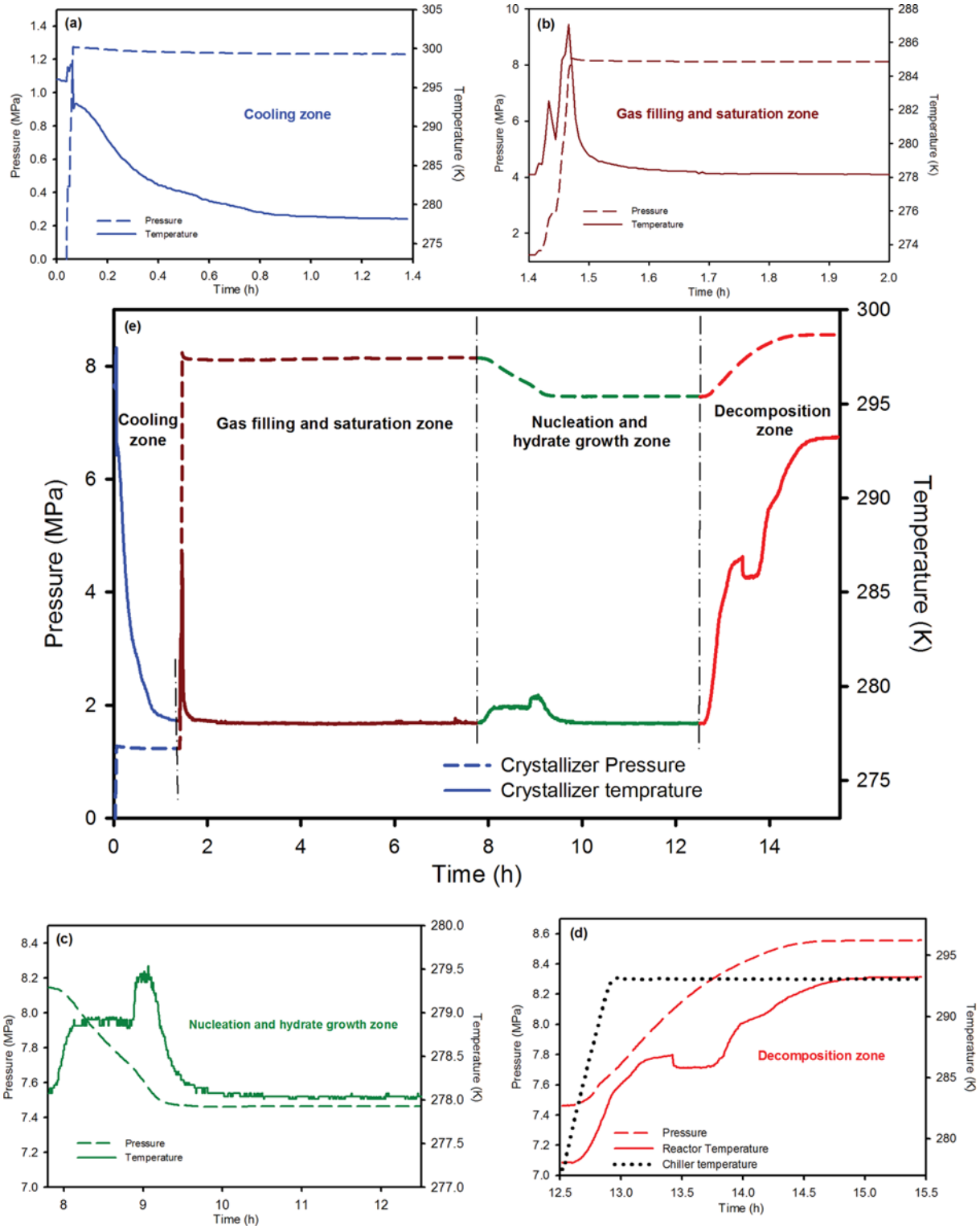


Fig. 1. Typical P-T profile and different zones during the morphology experiment.

of 278.2 K as shown Fig. 1(a). Once the cooling step was complete, the next step involved pressurizing the crystallizer to 8.0 MPa (experimental pressure). During the pressurization phase, there is a rise in temperature observed as shown in the enlarged gas filling and saturation zone represented in Fig. 1(b). This temperature peak is due to the increasing gas pressure in the crystallizer after which the temperature gradually lowers and reaches the experimental temperature in about 5-10 min. Note that after the pressurization step there is no significant pressure drop caused by the dissolution of methane in water due to the quiescent state and the low solubility of methane in water, and hence the crystallizer remains in this zone until hydrate nucleation occurs in the crystallizer. Exothermic nature of hydrate formation results in the temperature peak and a pressure drop (due to gas consumption or gas enclathration into the hydrate cages). As can be seen in Fig. 1(c) from the enlarged nucleation and hydrate formation zone (C) presented that about 1.5 K temperature rise and total pressure drop of about 0.7 MPa was observed during the hydrate formation step. There is a steady temperature profile after the initial temperature spike for about 45 min followed by further temperature rise before cooling down to the experimental temperature. The thermocouple location is at the center of the column/hollow silica bed and as detailed in the next section, hydrate growth initially predominantly occurs along the walls of the column followed by the growth at the center; thus the steady temperature profile might be due to the hydrate growth along the wall, and as the hydrate growth happens at close proximity to the thermocouple a peak could be distinctly observed followed by the lowering of the temperature to the set experimental temperature.

Once the hydrate formation process was complete, no further pressure drop could be observed in the crystallizer and the temperature had reached the original experimental temperature of 278.2 K. Sufficient time was given such that the pressure was stable. After this, the hydrates formed were dissociated employing thermal stimulation by increasing the crystallizer temperature to 293.2 K, thus a 15 K temperature rise was provided to decompose the hydrates. It took about 25 min for the chiller to reach the dissociation temperature when the set point was changed from 278.2 K to 293.2 K. The chiller temperature profile is included in Fig. 1(d). The decomposition zone (D) presented clearly shows the increase in temperature along with the increasing pressure due to the release of gas from hydrate cages. There is a small drop in the temperature about 0.9 h after start of decomposition that could be due to the detachment of the hydrate lump attached to the thermocouple, which will be discussed in detailed in Fig. 3 of this manuscript. The final pressure of the crystallizer is about 8.5 MPa, which is higher than the experimental pressure of 8.0 MPa due to the thermal expansion of gas due to heating from 278.2 K to 293.2 K. Decomposition is observed to be complete when both temperature and pressure of the crystallizer stabilize. After the first formation/dissociation cycle, the gas was vented completely and then the crystallizer was cooled to experimental temperature (278.2 K). After a standby time of 2 h, the crystallizer was pressurized to the experimental pres-

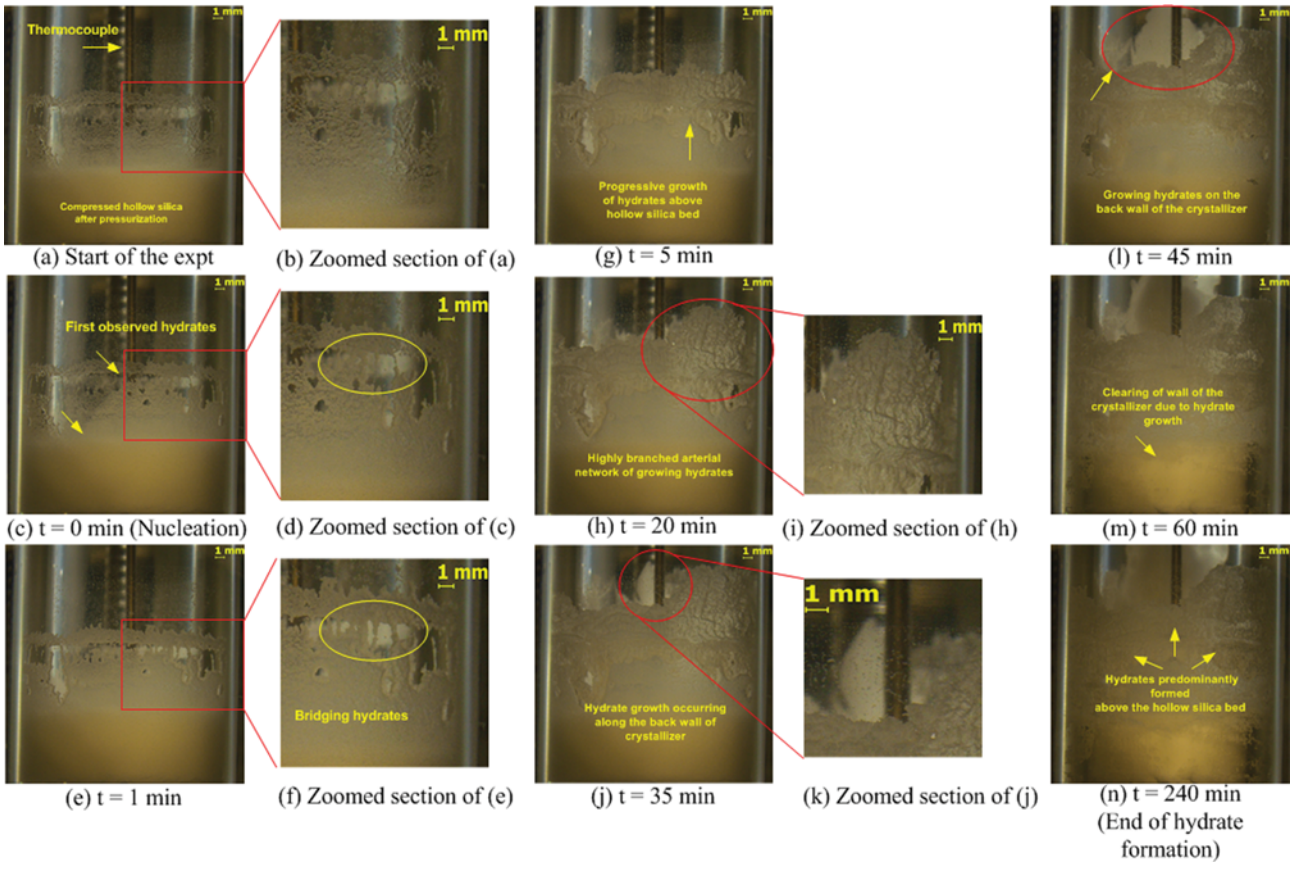


Fig. 2. Morphology of methane hydrates during the formation experiment in the hollow silica bed with 1 : 8 ratio of hollow silica to water.

sure of 8.0 MPa again for the conduction of memory experiment. Memory experiment refers to the experiment in which the water that had previously formed hydrates was subjected to hydrate formation once again. The memory experiment was conducted to ensure the consistency of gas uptake performance in repeated cycles using the same hollow silica bed.

RESULTS AND DISCUSSION

SEM and TEM images of hollow silica powder at different magnifications are provided in supporting information as Fig. S2 and Fig. S3, respectively. SEM image shows the spherical hollow silica particles in the range of 30-70 μm. TEM image (Fig. S3) shows that hollow silica used has a hollow core surrounded by a thin shell making it very light and less dense, enabling it to easily float in water.

1. Morphology of Methane Hydrate Formation in Hollow Silica

Fig. 2 presents the morphology of methane hydrates in the hollow silica bed during the hydrate formation experiment with hollow silica-to-water ratio of 1 : 8. Fig. 2(a) shows the initially set silica bed at experimental conditions with few wet hollow silica particles seen on the crystallizer wall as described earlier. Fig. 2(c) shows the nucleation of hydrates with a section of wetted silica near the interface turning to hydrates; the demarcation between hydrated and non-hydrate zone is indicated by arrows. For clarity, we have presented images 2(b) and 2(d). Fig. 2(b) clearly shows watery and wetted silica particles attached to the column above the bed, whereas in Fig. 2(d) water in those particles have transformed into hydrate that can be easily discernible above the hollow silica bed. Thus there is a zone of hydrates observed rather than independent single hydrate crystals. 1 min after nucleation all wetted hollow silica particles near the gas/hollow silica bed interface were converted to hydrates (Fig. 2(e)). The "bridge-effect" and growth of hydrates as explained by Beltran and Servio [52] was observed during this period. Encircled regions in the zoomed Figs. 2(d) and 2(f) stand as distinctive proof of the bridge effect. There are no prominent connections between the hydrates in Fig. 2(d), yet after a minute, hydrates are seen to be well-connected and tend to form a bridge like structures as seen in circled region in Fig. 2(f). Following this, hydrates are observed to grow progressively above the gas/silica bed interface into the gas phase (Fig. 2(g)-(n)). Fig. 2(i) shows a zoomed section during the growth of hydrates wherein a highly branched arterial network of hydrate structure is observed. This network might have enabled the water dispersed in the hollow silica bed to rise and form methane hydrates above the bed. The hydrate growth above the gas/silica bed interface occurs throughout the entire bed; prominent growth of hydrates along the back wall of the crystallizer was first observed 25 min after nucleation (Fig. 2(j)). The zoomed section presented in Fig. 2(k) clearly shows the dense white hydrates visible on the back wall of the crystallizer, which further intensifies subsequently (Fig. 2(l)-(m)). Hydrates were observed to grow dense, and 60 min following nucleation, clearing of the crystallizer wall in the section front of hollow silica bed was observed (Fig. 2(m)). Probable reason for this clearing could be the movement of water from the silica bed to the gas-hydrate interface for further hydrate growth and densification/drying up of hydrates. We believe that owing to the small pore spaces (in the order of few microns) and the presence of highly interconnected pore spaces (due to high porosity) had resulted in the formation of "capillary channels" that had caused the migration of water dispersed in the silica bed to rise above the bed to the gas interface, after which they get converted to hydrates. When most of the water had been transported and hydrates had grown dense there seems to be a localized clearing observed on the crystallizer wall (Fig. 2(m)). Fig. 2(n) shows the morphology of methane hydrates formed from the hollow silica bed 4 h after the nucleation.

Formation of methane hydrates above the hollow silica bed is quite different than that observed in earlier study using sand and activated carbon [53]. In the presence of silica sand both molecular level observations using an NMR micro imaging and macroscopic kinetics study under visual observation [53-56] revealed the formation of hydrates inside the interstitial pore space for methane hydrates. A few studies have reported the crystal growth of methane hydrates in silica sand [53,57,58]. Jin et al. [58] studied methane hydrate formation in sand with 20 wt% water saturation using optical microscopy and attenuated total reflection - infrared spectroscopy (ATIR-IR). They reported hydrate formation in porous media hydrate formation occurred in two discrete steps - the first step involved the formation of film like hydrates at the interstitial pore spaces followed by the second step cracking of the hydrate film resulting in increased water conversion to hydrates and cementing of the sand grains. Babu et al. [53] investigated methane hydrate formation in silica sand (0.14 cm^3/g pore volume) with 50% and 100% water saturation in pores. Growth of hydrate front originating from any random location inside the bed at different water saturations was observed in silica sand. Primarily, the hydrate formation occurred in the interstitial pore spaces available between the sand particles. In presence of low density hollow silica particles considered in hollow silica to water ratio of 1 : 8, hydrates predominantly formed above the hollow silica bed in the gas phase. Relatively small interstitial pore spaces in the hollow silica bed and the low density of the material facilitated the movement of water by capillary action along with a few hollow silica particles to the gas hydrate interface, resulting in formation of hydrates above the bed significantly rather than within the bed itself. It can be clearly inferred that majority of methane hydrates are formed above the hollow silica bed suggesting the formation of pure bulk methane hydrates. This ability of water to migrate from the interstitial pore spaces of hollow silica could be the reason for the fast kinetics reported in the literature recently.

2. Morphology of Methane Hydrate Dissociation in Hollow Silica

Decomposition of hydrates was then performed by thermal stimulation heating the crystallizer to 293.2 K; 15 K temperature rise was provided and the images during hydrate dissociation were recorded and presented in Fig. 3. Fig. 3(a) shows the hollow silica bed along with fully formed hydrates on the top at the start of decomposition experiment. About 25 minutes after the start of decomposition experiment, dense hydrates observed earlier tend to give a glossy appearance marking the start of dissociation as seen in Fig. 3(c). Zoomed section shown in Fig. 3(d) clearly shows the glossy hydrate layer in comparison to the dense hydrates that can be seen in the zoomed section of Fig. 3(b). 30 min after the start of decomposition small water droplets are seen on the crystallizer

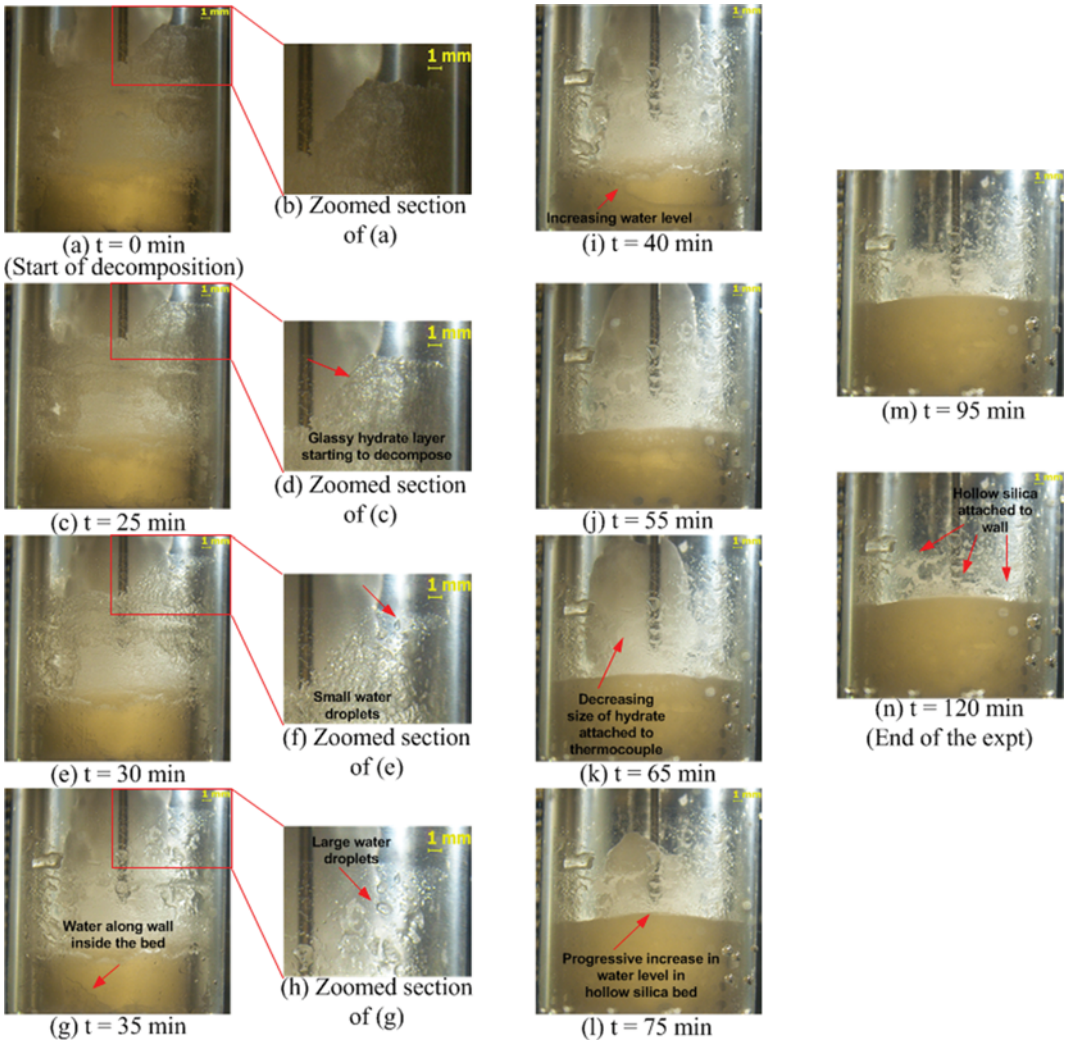


Fig. 3. Morphology of methane hydrates during the dissociation experiment in the hollow silica bed with 1 : 8 ratio of hollow silica to water.

wall (Fig. 3(e) with enlarged section presented in Fig. 3(f)). These small water droplets mature into larger droplets at 35 min after the start of decomposition experiment (Fig. 3(h)). Also, water was observed to collect along the wall at the bottom of the crystallizer column due to hydrate dissociation (Fig. 3(g)). The water level increases with the progress in time and covers the entire bed at about 55 minutes after the start of the decomposition experiment (Fig. 3(i)-(j)). A lump of methane hydrate was found attached to the thermocouple and its size reduced gradually due to the decomposition with the progress of time (Fig. 3(j)-(m)). The increased dissociation of the hydrate lump also corresponded to the increase of water level in the hollow silica bed. Dissociation experiment was complete when visually no hydrates were present in the bed and the crystallizer temperature/pressure stabilized. Fig. 3(n) shows the observation of silica bed after the completion of the dissociation experiment. Considerable hollow silica particles along with water are seen attached to the walls of the crystallizer after the dissociation experiment. These particles seem to be displaced from the bed during the hydrate formation as the outline of these particles maps the hydrate formation zone observed at the end of formation experiment (Fig. 2(n)). Light weight of these particles resulted in easy movement/transport of particles during the hydrate growth phase. Further, these particles seem to be aggregating and are evidently more in number after the completion of the dissociation experiment compared to few wetted silica particles observed along the wall above the bed at the start of formation experiment due to the compression of hollow silica bed during pressurization. Supporting information Fig. S4 provides the visual comparison between hollow silica particles present before the start of formation experiment and after the completion of dissociation experiment. For better understanding, videos showing the distinct morphology changes occurring during the formation (Video 1) and decomposition (Video 2) of methane hydrates using fresh water are included in the supporting information.

Fig. S5 in the supporting information shows the morphology of hollow silica bed along with pressure observed in the crystallizer during the venting process. It was observed that the entire column was covered with exhaustive amounts of the hollow silica particles after the completion of venting to the atmospheric pressure. We used an acrylic block to ensure that the entire silica bed was

within the area of observation by the microscope. This block tried to move up during venting due to the reduction of pressure as a result of which most of the column was covered with wetted hollow silica particles. We planned to conduct a 'memory' experiment using the same hollow-silica bed to evaluate the gas uptake performance and to observe the morphology of hydrates formed. This is essential for practical applications, wherein the porous medium has to be used for repeated cycles of hydrate formation/dissociation without showing significant deterioration in performance. "Memory" refers to the experimental trial in which hydrates are formed successively using the same water+hollow silica bed that had already formed hydrates. After dissociation and venting, the hollow silica bed was cooled to the experimental temperature and pressurized to 8 MPa once again for the hydrate formation. Images of the hollow silica bed observed during hydrate formation and dissociation of the memory experiment conducted are presented in Figs. S6 and S7 of the supporting information, respectively. Nucleation occurred quickly at around 15 min after the start of memory experiment in comparison to around 6.4 h of induction time for the fresh experiment. This was expected as the memory experiment had resulted in faster nucleation for other natural gas hydrates systems reported in the literature [31,59]. Overall, except for the reduced clarity of hydrate growth due to the extensive wetted hollow silica particles, the hydrate formation was similar to that of the fresh experiment, including gas uptake and water to hydrate conversion that will be discussed later in the section on kinetics of hy- drate formation in hollow silica.

3. Morphology of Methane Hydrate Formation and Dissociation in Absence of the Thermocouple within the Hollow Silica Bed

In the fresh and memory experiments conducted, the thermocouple was kept touching the top layer of the hollow silica bed, due to which an additional surface was available for hydrates to grow, and hydrates were observed to attach to the thermocouple during the growth phase. To eliminate the effect of the thermocouple, we decided to conduct another next set of experiments at same experimental conditions with the thermocouple kept in the gas phase well above the bed, and observe the morphology changes during hydrate formation and dissociation experiments.

Fig. 4 shows the observation of hydrate formation experiment conducted in hollow silica bed without the thermocouple. Fig. 4(a) shows the hollow silica bed after pressurization before the hydrate formation. Fig. 4(c) shows the nucleation observed by the hydrates observed along the gas/hollow silica interface. Zoom section in Fig. 4(d) clearly depicts the nucleation of hydrate in comparison to the zoomed section in Fig. 4(b). Fig. 4(e)-(j) present the hydrate growth occurring after nucleation; initially a small lump of hydrate was seen to be protruding from the gas/hollow silica interface (Fig. 4(f)), which later grew across the column (Fig. 4(h)) almost covering the entire column with hydrates (Fig. 4(j)). Progressive growth of hydrates above the hollow silica bed was observed (Fig. 4(k)-(n)), similar to formation experiments conducted with a thermocouple. Clearing of the crystallizer wall as discussed earlier was also observed 15 minutes after the nucleation (Fig. 4(l)). Progressive

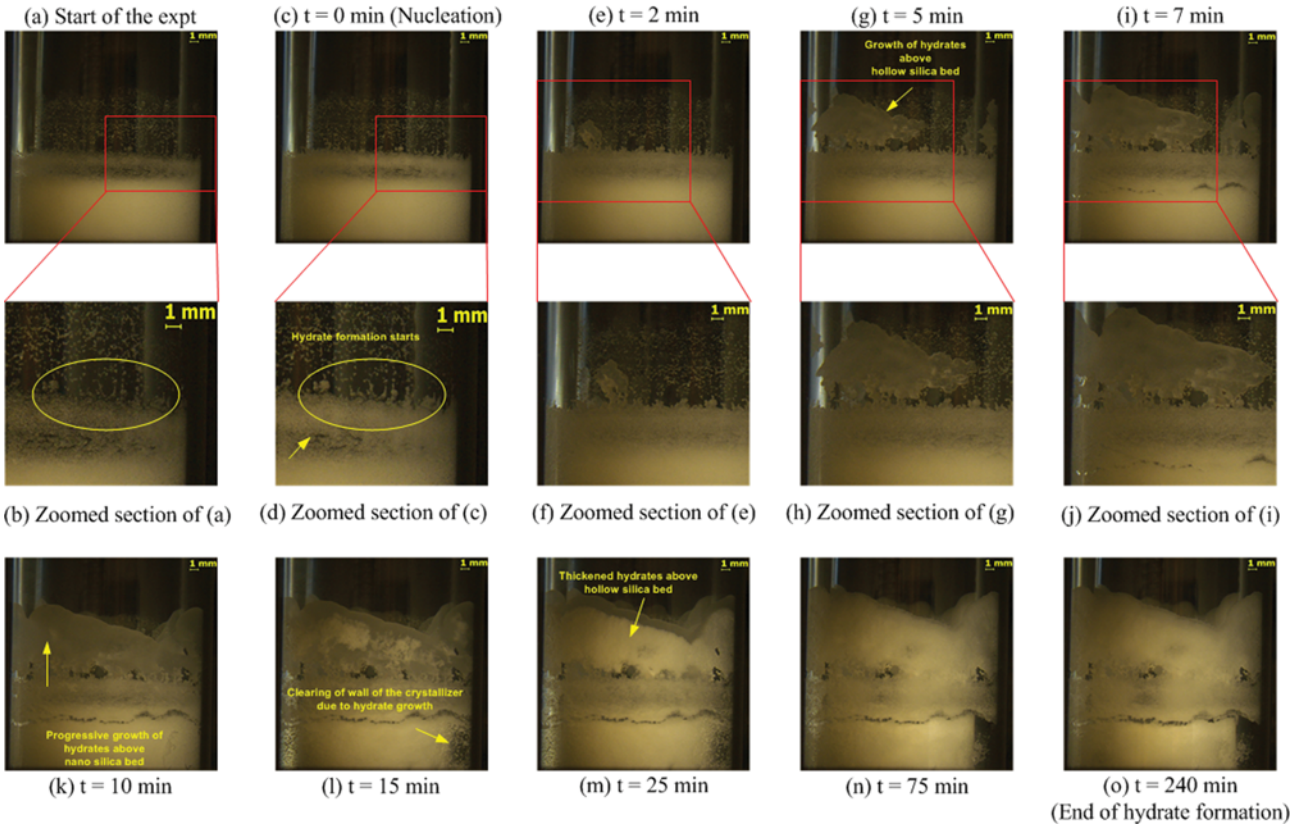


Fig. 4. Morphology of methane hydrates during the formation experiment without thermocouple in the hollow silica bed.

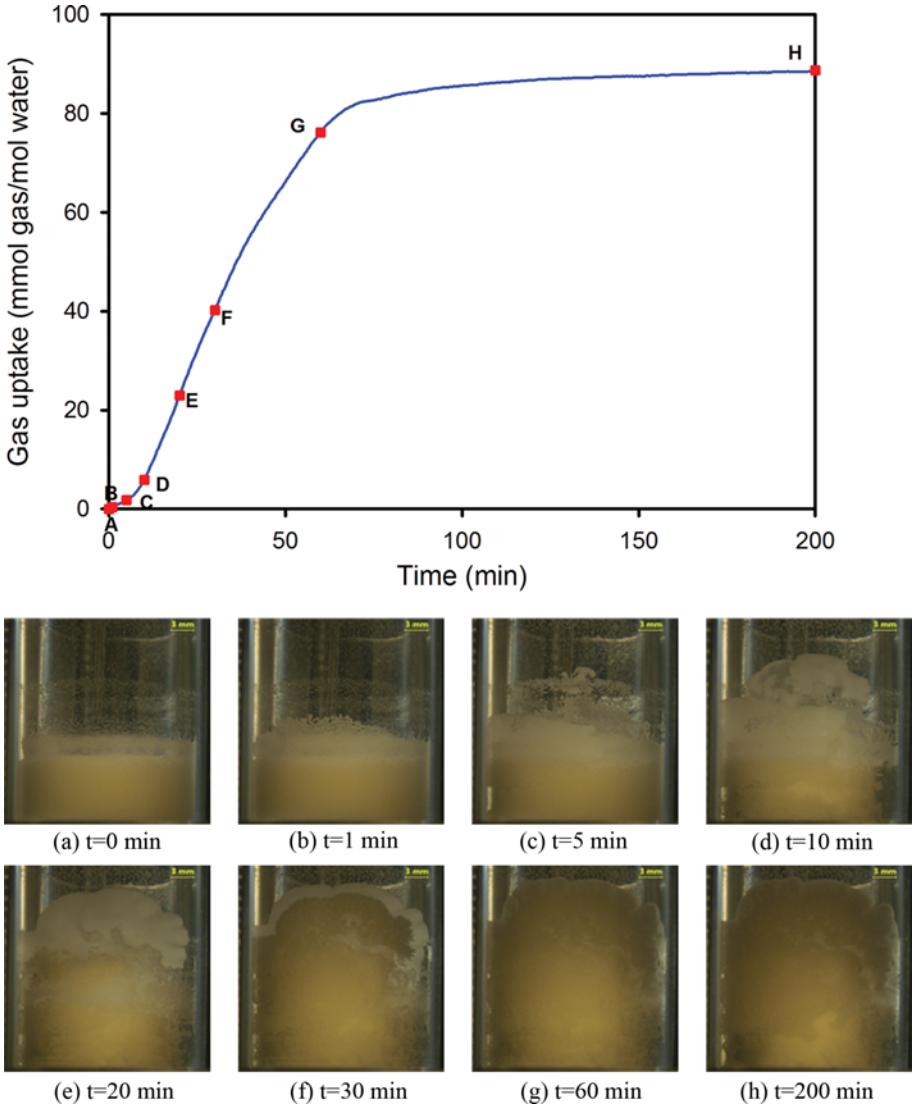


Fig. 5. Typical gas uptake profile of experimental trial using 1 : 8 ratio of hollow silica to water along with mapped morphology images at specific time intervals.

thickening of the hydrates formed above the hollow silica bed occurred (Fig. 4(l)-(n)). Cracks that first occurred in the hollow silica bed (Fig. 4(i)) widened slightly with the progressive growth and thickening of hydrates (Fig. 4(k)-(o)). The final image after the completion of hydrate formation is shown in Fig. 4(o). Video showing the morphology changes during the formation of methane hydrates in hollow silica bed without the thermocouple is provided in the supporting information (Video 3).

Following this, dissociation of hydrates was performed by thermal stimulation and the morphology changes that happened are presented in Fig. S8 of the supporting information. From these morphology observations, it can be concluded that the presence or absence of a thermocouple did not affect the morphology of hydrate formation and decomposition with methane hydrates predominantly formed as bulk hydrates above the hollow silica bed. Note that for a surfactant containing systems, the study by Yoslim et al. [60] showed that the presence of thermocouple had a significant effect on hydrate nucleation and hydrate growth morphology.

4. Gas Uptake and Morphology of Methane Hydrate Formation with Varying Ratios of Hollow Silica to Water

Fig. 5(top) shows a typical gas uptake profile for fresh experiment trial F3 with thermocouple touching the hollow silica bed. Selected points ((a)-(h)) are presented on the gas uptake profile, and the mapped morphology of hollow silica bed at these points is provided in the bottom of Fig. 5. There is clearly significant hydrate formation and growth above the hollow silica bed in 30 min from nucleation (points (a) to (f)). Further, after 60 min from nucleation (point (g)), the hydrate growth is almost complete and no further significant morphology change occurs even after long time of 240 min from nucleation (point (h)). Interestingly, point (g) is quite close to t_{90} (time taken for 90% completion of hydrate formation) of 68.3 min, which signifies 90% completion of hydrate formation. Thus, the morphology of growing hydrates observed in hollow silica bed correlates well with kinetic data recorded and explained

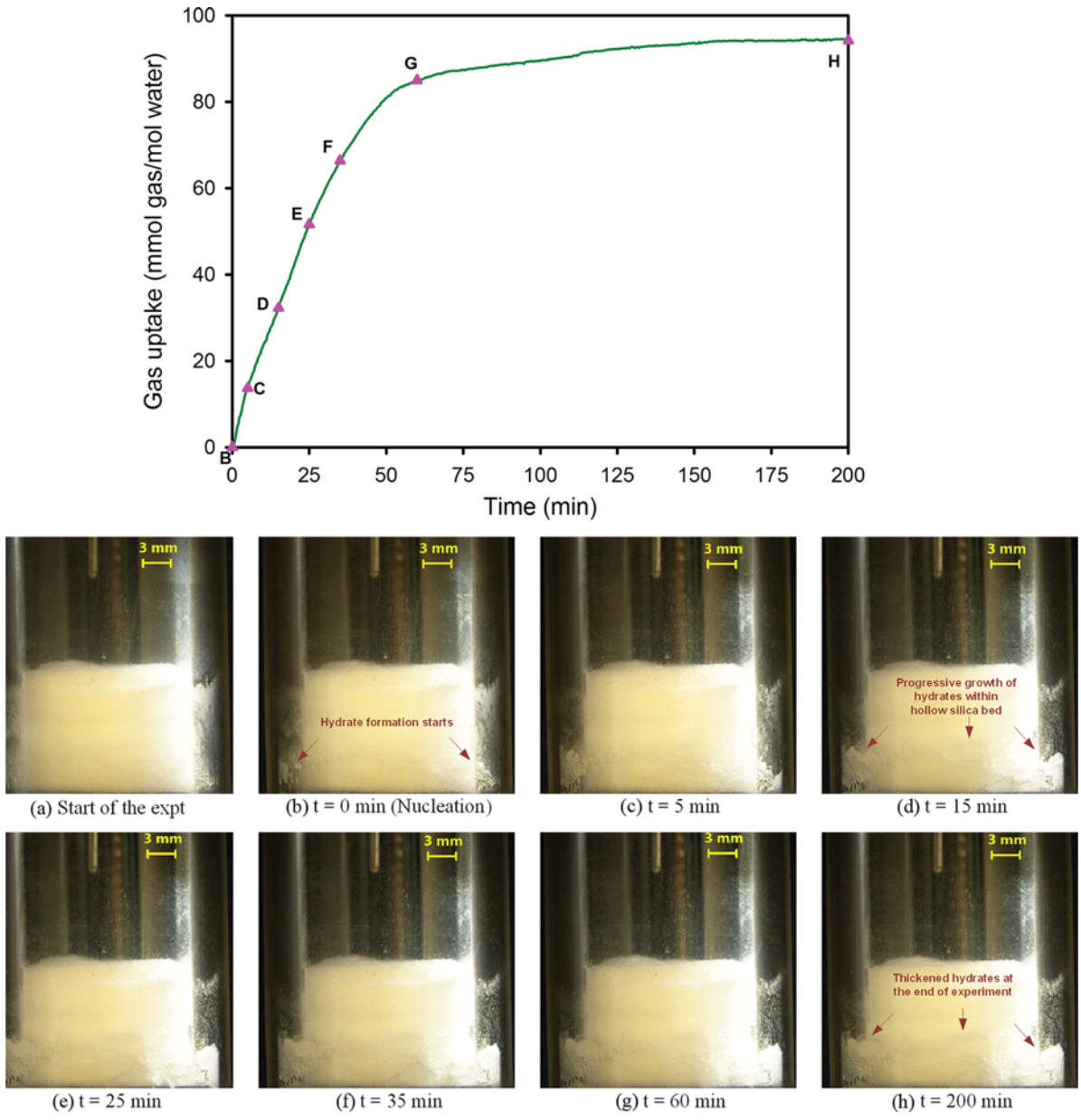


Fig. 6. Typical gas uptake profile of experimental trial using 1 : 4 ratio of hollow silica to water along with mapped morphology images at specific time intervals.

in the previous section.

We also performed methane hydrate formation/dissociation experiments with other hollow silica to water ratios of 1 : 4 and 1 : 6. Figs. 6 and 7 present the morphology of methane hydrates along with corresponding gas uptake profiles formed at these two ratios, respectively. From Fig. 6(a)-(h) it can be clearly observed that methane hydrates are completely formed within the bed when 1:4 ratio of hollow silica to water was considered for hydrate formation. No hydrate growth was observed above the hollow silica bed and predominant hydrate growth occurred at the bottom of the bed. Gas uptake profile was also similar to the previous experiment at 1 : 8 silica to water ratio with t_{90} of 60.5 min. Fig. 7 presents the gas uptake profile along with morphology of methane hydrate formation observed for the experiment conducted with hollow silica to water ratio of 1 : 6. With the increase of water, it is evident from the figure that that there is minimal methane hydrate formation observed above the hollow silica and maximal methane hydrate formation within the bed. Thus, there exists critical hollow silica-to-water ratio beyond which there is predominant hydrate formation above the hollow silica bed. 1 : 6 ratio could be this critical ratio as we can observe predominant hydrate formation above the bed at higher water content (1 : 8 hollow silica to water ratio) and predominant hydrate formation within the bed (with no hy- drate formation above the bed) for lower water content (1 : 4 hollow silica to water ratio). Clearing of hydrates from the walls similar to that observed for 1 : 8 experiments can be seen in Fig. 7(h).

Fig. 8 presents a bar chart of gas uptake and the normalized rate of hydrate formation (NR_{20}) along with error observed for

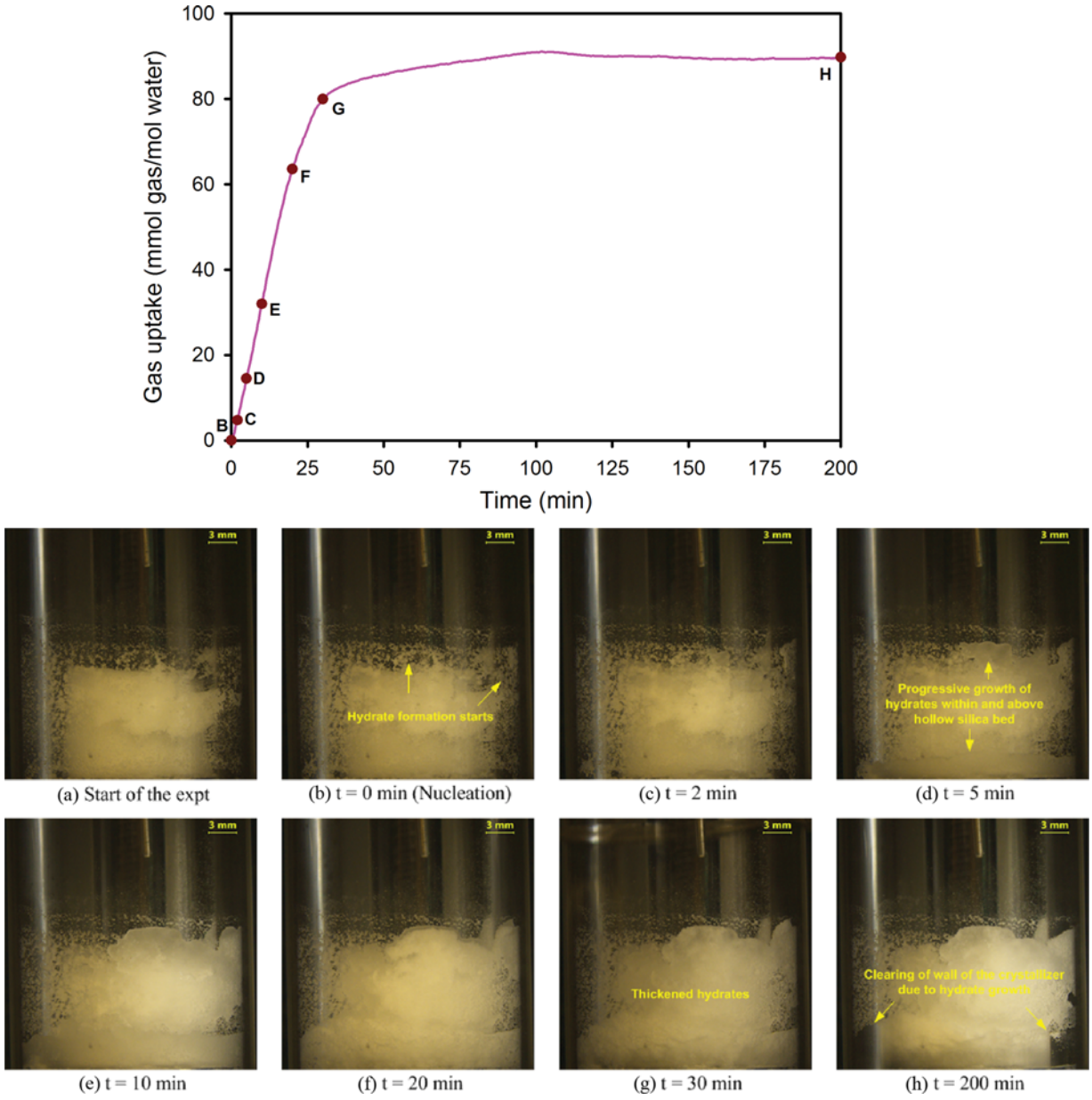


Fig. 7. Typical gas uptake profile of experimental trial using 1 : 6 ratio of hollow silica to water along with mapped morphology images at specific time intervals.

experiments conducted at varying ratios of hollow silica to water. NR_{20} is the normalized rate of hydrate growth (in mol min^{-1} m^{-3}) calculated by best fit obtained from the plot of the average gas uptake due to hydrate growth at each experimental condition against time for the first 20 minutes after nucleation. 20 minutes duration gave the best fit for rate quantification with R^2 values of 0.985, 0.999 and 0.996 for experiments with 1 : 4, 1 : 6 and 1 : 8 ratios of hollow silica to water, respectively.

Interestingly, from Fig. 8, the total methane gas uptake (in terms of mmol of gas/mol of water) observed using different ratios of hollow silica to water remains similar in the range of 88 to 95 mmol of methane/mol of water despite the difference in morphology observed varying the water content in hollow silica bed. However, NR_{20} differs for each of the experiments conducted, the highest value being observed for the experiment with hollow silica to water ratio 1 : 6 where hydrate growth is observed both within the hollow silica bed and to a small extent above the bed. The experiment conducted with hollow silica to water ratio of 1 : 4 showed lower NR_{20} than the experiment with hollow silica to water ratio of 1 : 6 probably due to the entire hydrate formation only occurring within the hollow silica with only less water (2 ml) dispersed in the bed that might impose an impedance for the gas to access the water available for hydrates. NR_{20} for 1 : 8 ratio experiments was observed to be the least amongst the three ratio experiments conducted despite the enhanced hydrate growth observed above the hollow silica bed being probably due to the increased mass transfer resistance for the water to be transported from the bed to the gas/hydrate interfacial area for continued hydrate growth. Also, the amount of water

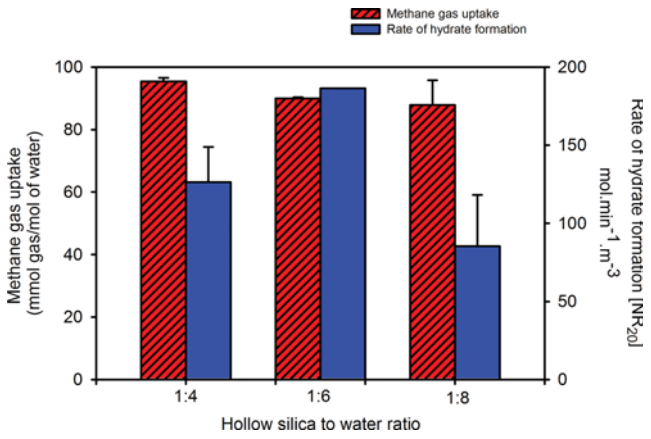


Fig. 8. Bar chart of total gas uptake and normalized rate of experimental trials conducted using different ratios of hollow silica to water along with error bars.

considered for hydrate formation in this case was the highest (4 ml) in comparison to other ratio experiments performed. Fig. 9 demonstrates schematically the difference in morphology before and after hydrate formation for the different ratios of hollow silica to water experimented.

5. Hydrate Formation Mechanism

From morphology observations, a schematic for the mechanism of hydrate formation for hollow silica to water ratio of greater than 1 : 6 is proposed and presented in Fig. 10. After the start of experiment, the nucleation or the formation of first hydrate crystal either occurred at the gas/hollow silica interface or within the bed. Hydrate crystals then started to grow utilizing the water in the hollow silica bed. Water was believed to be transported to the interface from the hollow silica bed through network of capillary channels formed due to highly interconnected micron sized pores. Increased water available at the interface resulted in bulk hydrate formation above the hollow silica bed. Some hollow silica particles move along the direction of forming hydrates due to their light weight. When substantial bulk hydrates form above the hollow silica bed, it becomes difficult for the remaining water to reach the gas/hydrate interface for further hydrate formation that resulted in completion of hydrate formation with certain percentage of unconverted water present in the hollow silica bed. Decomposition of hydrates by thermal stimulation resulted in the regeneration of hollow silica bed with water. However, hollow silica particles transported during hydrate formation remain attached to the wall of the crystallizer wetted with water. Thus there will be some loss of hollow silica during each hydrate formation/dissociation cycle.

Hydrate formation mechanism for experiments with hollow silica to water ratios of 1 : 4 or less was predominantly in the interstitial pore spaces and contained within the bed as reported in literature for other porous materials [37,53,58]. Kinetics of methane hydrate formation in hollow silica bed observed for the 1 : 8 hollow silica to water ratio was fitted using the well-known classical crystallization Avrami model for phase change. Experimental gas uptake values are well predicted by the Avrami model, as very good fit is observed for the first 30 minutes from nucleation. Beyond this time the model predictions deviate from the experimental data.

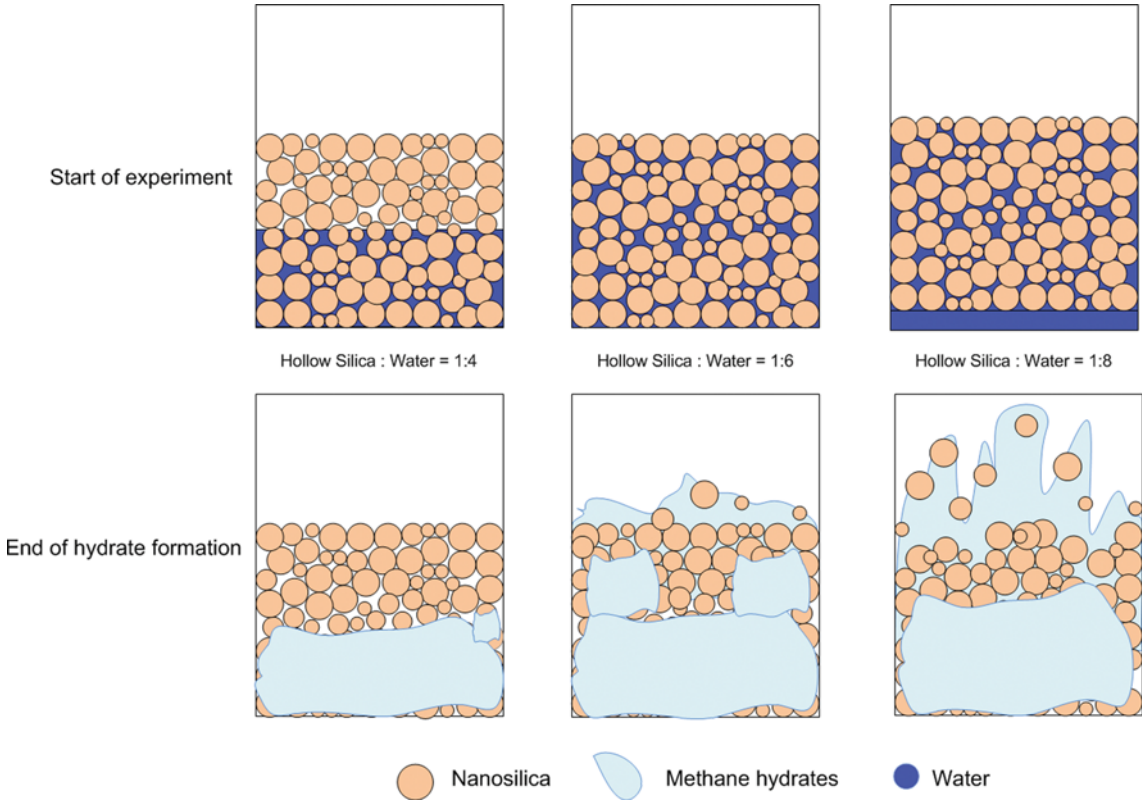


Fig. 9. Schematics of morphology observed before and at the end of experiment for different ratios of hollow silica to water.

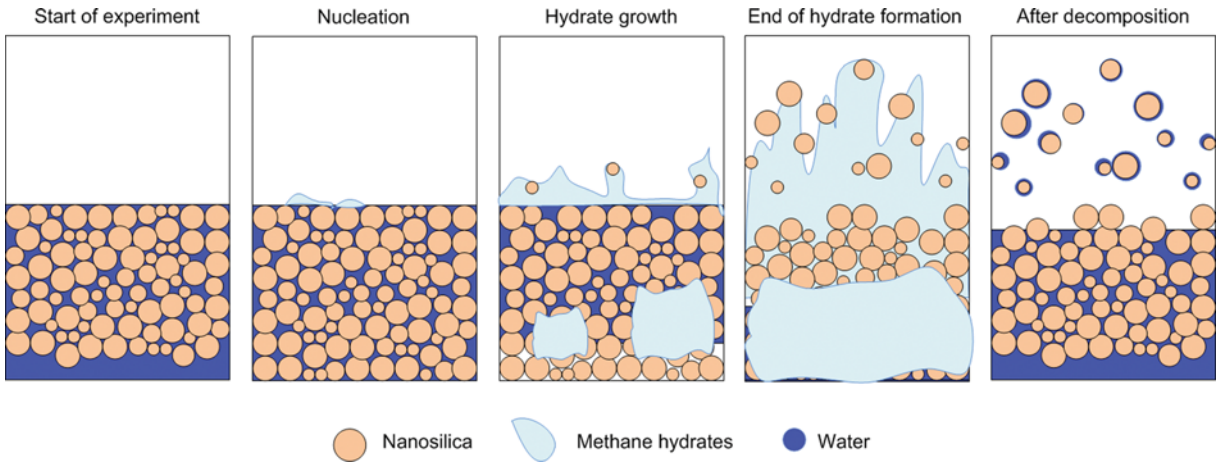


Fig. 10. Hydrate formation mechanism in the hollow silica bed using 1 : 8 ratio of hollow silica to water.

Detailed description of the Avrami model fit is included in the supporting information section S1 and Fig. S9.

CONCLUSION

We have elucidated the mechanism of methane hydrate formation/dissociation occurring in a light weight, hollow silica bed at different ratios of hollow silica to water. It is observed that extensive hydrate growth occurs on the top of hollow silica bed in the gas phase region beyond 1 : 6 critical ratio of hollow silica to water. This may aid in the easier separation of hydrates from the hollow silica bed for eventual natural gas storage and transport application. Below this critical ratio, hydrate formation was observed to be only within the hollow silica bed. Gas uptake (mmol of gas/mol of water) was observed to be similar despite the difference in morphology observed for different ratios of hollow silica to water. Our study revealed that thermal stimulation is the best dissociation approach if a light weight hollow silica medium is used. Our work also highlights some engineering challenges during dissociation that need to be mitigated for the usage of light weight hollow materials as porous media for natural gas storage and transport employing the clathrate hydrate process.

ACKNOWLEDGEMENTS

The financial support from the National University of Singapore (R-279-000-420-750, R-261-508-001-646 and R-261-508-001-733) is greatly appreciated. Dr. PSR Prasad would like to thank the Director of the National Geophysical Research Institute in Hyderabad for his constant encouragement and support. Dr. PSR Prasad further acknowledges GEOSCAPE project of NGRI under the 12th Five Year Scientific Program of CSIR for financial support.

SUPPORTING INFORMATION

SEM and TEM images of hollow silica (Fig. S2 and S3), characteristic observations of hollow silica bed during the conduction of morphology experiments (Fig. S1, S4 and S5), hydrate formation/dissociation of methane hydrates formed during the memory experiment (Fig. S6 and S7), hydrate dissociation observed in hollow silica bed without thermocouple (Fig. S8) and Avrami model fit for the gas uptake included in Section S1 and Fig. S9 of the Supporting information. Videos (Video 1 and Video 2) showing methane hydrate formation and dissociation with the thermocouple in hollow silica and Video 3 showing methane hydrate formation in hollow silica without the thermocouple are also included.

Additional information as noted in the text. This information is available via the Internet at http://www.springer.com/chemistry/journal/11814.

REFERENCES

1. D. Kurumov, G. Olchowy and J. Sengers, *Int. J. Therm.*, **9**(1), 73 (1988).
2. D. G. Friend, J. F. Ely and H. Ingham, *J. Phys. Chem. Reference Data*, **18**(2), 583 (1989).
3. Joint Research Centre (JRC), E.C., *Liquefied Natural Gas: Advantages And Drawbacks*, in *ScienceDaily* (2009).
4. N. Kirillov, *Chem. Pet. Eng.*, **40**(7), 401 (2004).
5. P. Englezos and J. Lee, *Korean J. Chem. Eng.*, **22**(5), 671 (2005).
6. Y. Song, et al., *Appl. Energy*, **145**, 265 (2015).
7. Z. R. Chong, et al., *Appl. Energy*, **162**, 1633 (2016).
8. P. Babu, et al., *Energy*, **85**, 261 (2015).
9. V. V. Struzhkin, et al., *Chem. Reviews*, **107**(10), 4133 (2007).
10. H. P. Veluswamy, R. Kumar and P. Linga, *Appl. Energy*, **122**, 112 (2014).
11. P. Babu, R. Kumar and P. Linga, *Chem. Eng. Sci.*, **117**, 342 (2014).
12. D. W. Davidson, *Water: A Comprehensive Treatise*, Clathrate hydrates, New York, Plenum Press, 2 (1973).
13. P. Englezos, *Ind. Eng. Chem. Res.*, **32**(7), 1251 (1993).
14. E. D. Sloan and C. A. Koh, *Clathrate hydrates of natural gases*, CRC Press (2008).
15. R. Boswell and T. S. Collett, *Energy Environ. Sci.*, **4**(4), 1206 (2011).
16. C. A. Koh, A. K. Sum and E. D. Sloan, *J. Natural Gas Sci. Eng.*, **8**, 132 (2012).
17. G. J. Moridis, et al., *SPE Reserv. Eval. Eng.*, **12**(5), 745 (2009).

18. H. Kanda, *Economic study on natural gas transportation with natural gas hydrate (NGH) pellets*, in *23rd World Gas Conference*, Amsterdam (2006).
19. T. Nogami, et al., *Development of natural gas ocean transportation chain by means of natural gas hydrate (NGH)*, in *Fifth International Conference on Gas Hydrates*, Trondheim, Norway (2005).
20. J. Gudmundsson, V. Andersson and O. Levik, *Gas storage and transport using hydrates*, in *Compendio de la Conferencia Mediterránea Marina* (1997).
21. J. S. Gudmundsson, M. Parlaktuna and A. Khokhar, *SPE Production and Facilities*, **9**(1), 69 (1994).
22. L. A. Stern, et al., *The J. Phys. Chem. B*, **105**(9), 1756 (2001).
23. P. S. R. Prasad and V. D. Chari, *J. Natural Gas Sci. Eng.*, **25**, 10 (2015).
24. K. Watanabe, S. Imai and Y. H. Mori, *Chem. Eng. Sci.*, **60**(17), 4846 (2005).
25. Y. Liu, et al., *Energy Technol.*, n/a-n/a (2015).
26. S. Lee, et al., *The J. Phys. Chem. C*, **111**(12), 4734 (2007).
27. J. S. Zhang, S. Lee and J. W. Lee, *Ind. Eng. Chem. Res.*, **46**(19), 6353 (2007).
28. H. P. Veluswamy, et al., *Chem. Eng. Sci.*, **132**, 186 (2015).
29. K. Okutani, Y. Kuwabara and Y. H. Mori, *Chem. Eng. Sci.*, **63**(1), 183 (2008).
30. H. Ganji, et al., *Fuel*, **86**(3), 434 (2007).
31. P. Linga, et al., *Int. J. Greenhouse Gas Control*, **4**(4), 630 (2010).
32. R. Susilo, *Methane storage and transport via structure H clathrate hydrate*, UNIVERSITY OF BRITISH COLUMBIA (Vancouver (2008).
33. R. Ohmura, et al., *Energy Fuels*, **16**(5), 1141 (2002).
34. H. P. Veluswamy, et al., *Chem. Eng. J.*, **290**, 161 (2016).
35. S.-P. Kang, Y. Seo and W. Jang, *Energy Fuels*, **23**(7), 3711 (2009).
36. L. Yang, et al., *Ind. Eng. Chem. Res.*, **50**(20), 11563 (2011).
37. A. Siangsai, et al., *Chem. Eng. Sci.*, **126**, 383 (2015).
38. A. Siangsai, et al., *Improved methane hydrate formation rate using treated activated carbon and tetrahydrofuran*, **47**(4 SPEC. ISS.), 352 (2014).
39. A. Siangsai, et al., *Roles of activated carbon and tetrahydrofuran on methane hydrate phase equilibrium*, 1195 (2014).
40. B. O. Carter, et al., *Langmuir*, **26**(5), 3186 (2010).
41. J. Park, et al., *The J. Phys. Chem. C*, **119**(4), 1690 (2015).
42. W. Wang, et al., *J. Am. Chem. Soc.*, **130**(35), 11608 (2008).
43. J. Pasieka, S. Coulombe and P. Servio, *Chem. Eng. Sci.*, **104**, 998 (2013).
44. M. Cha, et al., *Chem. - An Asian J.*, **9**(1), 261 (2014).
45. S. Baek, J. Min and J. W. Lee, *RSC Adv.*, **5**(72), 58813 (2015).
46. P. S. R. Prasad, Y. Sowjanya and V. Dhanunjana Chari, *J. Phys. Chem. C*, **118**(15), 7759 (2014).
47. V. D. Chari, et al., *J. Natural Gas Sci. Eng.*, **11**, 7 (2013).
48. P. S. R. Prasad, *J. Chem. Eng. Data*, **60**(2), 304 (2015).
49. V. D. Chari, et al., *Energy Fuels*, **27**(7), 3679 (2013).
50. H. P. Veluswamy, T. Yang and P. Linga, *Cryst. Growth Des.*, **14**(4), 1950 (2014).
51. T. Nakamura, et al., *Chem. Eng. Sci.*, **58**(2), 269 (2003).
52. J. G. Beltrán and P. Servio, *Cryst. Growth Des.*, **10**(10), 4339 (2010).
53. P. Babu, et al., *Energy Fuels*, **27**(6), 3364 (2013).
54. P. Mekala, et al., *Energy Fuels*, **28**(4), 2708 (2014).
55. C. Haligva, et al., *Energy Fuels*, **24**(5), 2947 (2010).
56. P. Linga, et al., *Energy Fuels*, **23**(11), 5496 (2009).
57. J.-W. Jung and J. C. Santamarina, *J. Cryst. Growth*, **345**(1), 61 (2012).
58. Y. Jin, Y. Konno and J. Nagao, *Energy Fuels*, **26**(4), 2242 (2012).
59. P. Linga, R. Kumar and P. Englezos, *Chem. Eng. Sci.*, **62**(16), 4268 (2007).
60. J. Yoslim, P. Linga and P. Englezos, *J. Cryst. Growth*, **313**(1), 68 (2010).

Supporting Information

Mechanism of methane hydrate formation in the presence of hollow silica

Hari Prakash Veluswamy*, Pinnelli Seetha Rama Prasad, and Praveen Linga*,†**

*Department of Chemical and Biomolecular Engineering, National University of Singapore, Singapore 117 585, Singapore
**Gas Hydrate Division, National Geophysical Research Institute, Council for Scientific and Industrial Research, Uppal Road, Hyderabad 500 007, India
(*Received 5 October 2015 • accepted 4 February 2016*)

S1. Avrami model for methane gas uptake for 1 : 8 ratio of hollow silica to water experiments

Kinetics of methane hydrate formation in hollow silica bed was fitted using the well-known classical crystallization Avrami model for phase change [1-3]. The model equations are presented in Eqs. (1) and (2)

$$\alpha = 1 - \exp(-k(t)^n) \quad (1)$$

$$\ln[-\ln(1-\alpha)] = n \ln(t) + \ln(k) \quad (2)$$

where α in the model in previous works [4,5] refer to the water to hydrate conversion ratio at time t, but we have considered α to be the gas uptake at time t to correlate directly the gas uptake to the hydrate formation kinetics, k is the overall crystallization rate constant, n is the Avrami exponent which represents the hydrate nucleation and growth. 'n' and 'k' are obtained from slope and intercept of the line fit by plotting $\ln[-\ln(1-\alpha)]$ vs 't' as shown in Fig. S9a. The n value is obtained to be 1.19 and the k value is calculated to be $8.3*10^{-7}$ mmol of gas/mol of water·min^{-1}.

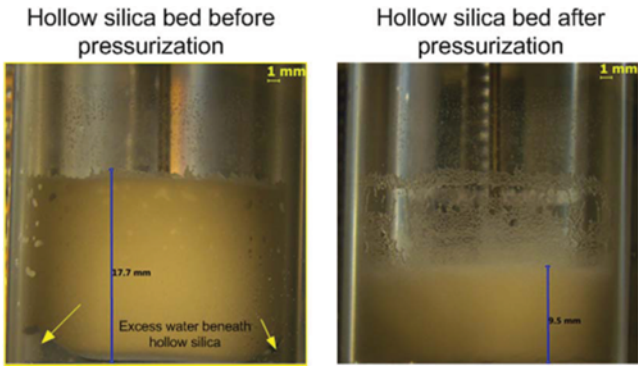


Fig. S1. Hollow silica bed before and after pressurization during the formation experiment using hollow silica to water ratio of 1 : 8.

First approximation of the avrami exponent, n is considered to be summation of n_d+n_n, where n_d is the dimensionality of the growing crystals and n_n indicates the time dependence of the nucleation. nd can have only integer numbers 1, 2 or 3 corresponding to one-, two- or threedimensional crystal growth. The value of nn should be either 0 or 1, where 0 corresponds to instantaneous nucleation where in nuclei appear all at once or 1 to sporadic nucleation wherein number of nuclei grow with time. However, since in many cases the nucleation may be in between completely instantaneous or completely sporadic, it can lead to non-integer value of n. Value of 1.19 in the present fit indicates one dimensional hydrate growth (n_d equal to 1) and fractional value of n_n signifying the system exists between instantaneous and sporadic nucleation events with nucleation occurring at different time intervals (shown by temperature profile in hydrate growth zone in Fig. 1). Experimental and avrami model predictions for gas uptake for the first 40 min from nucleation are shown in Fig. S9b. It can be observed from the figure that experimental gas uptake values are well predicted by the Avrami model as very good fit is observed for the first 30 minutes. Beyond this time the model predictions deviate from the experimental data.

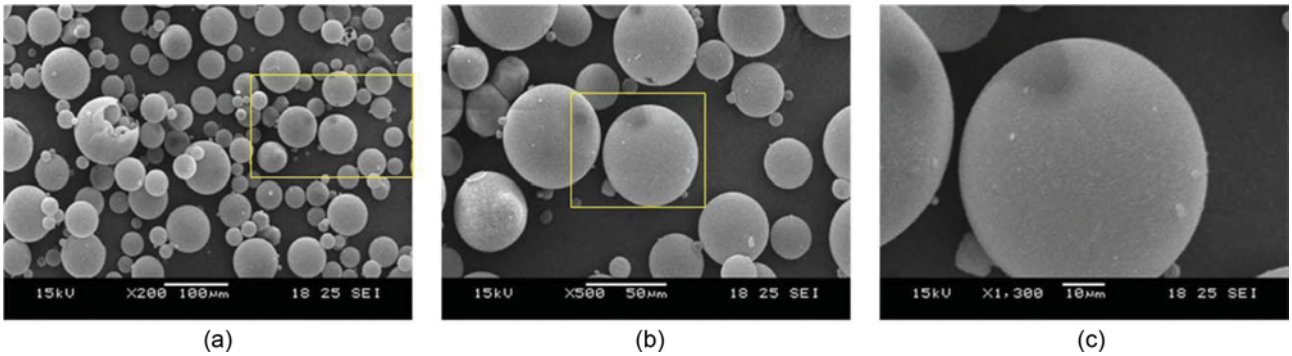


Fig. S2. SEM image of hollow silica at different magnifications.

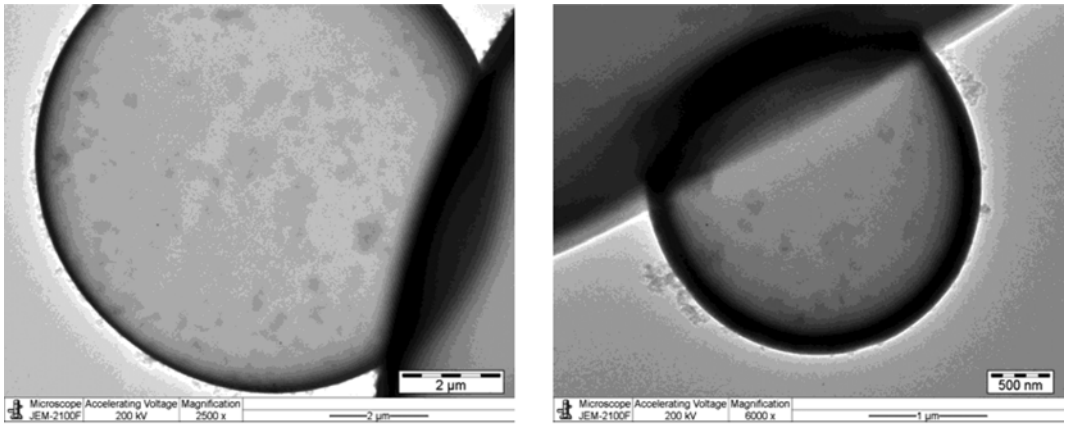


Fig. S3. TEM image of hollow silica.

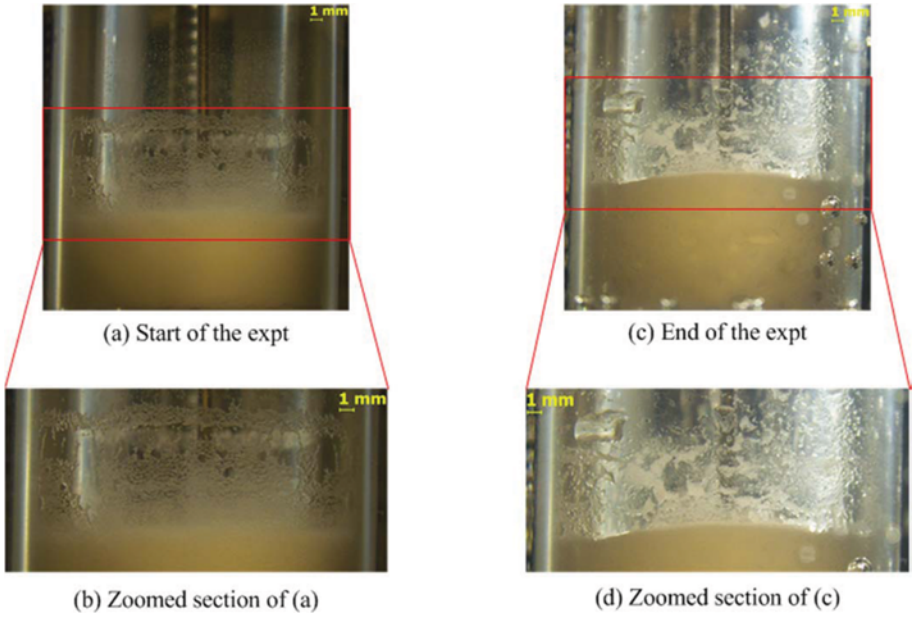


Fig. S4. Comparison of hollow silica on the column wall before and after the hydrate formation experiment using hollow silica to water ratio of 1 : 8.

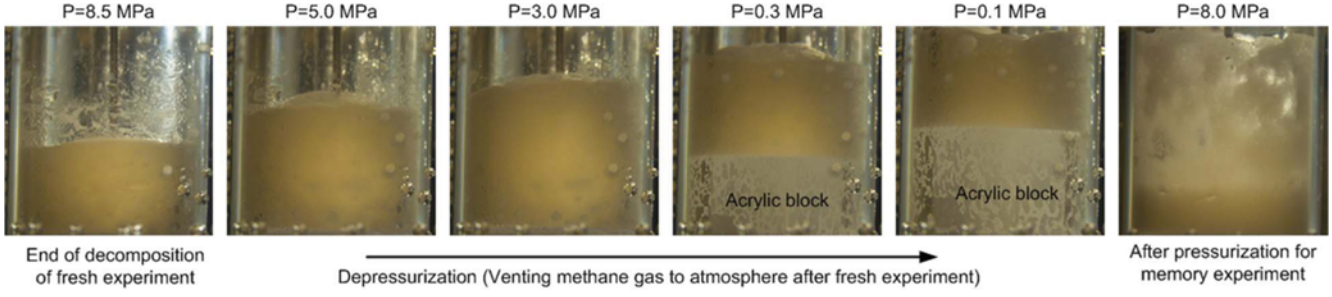


Fig. S5. Movement of hollow silica bed along with acrylic block during venting after the completion of dissociation of fresh experimental trial.

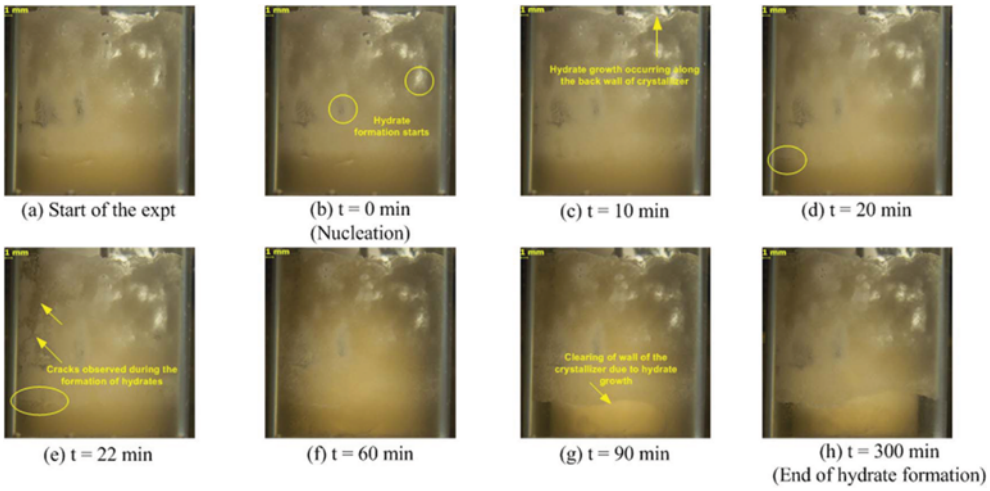


Fig. S6. Morphology of methane hydrates formation during the memory experiment in the hollow silica bed.

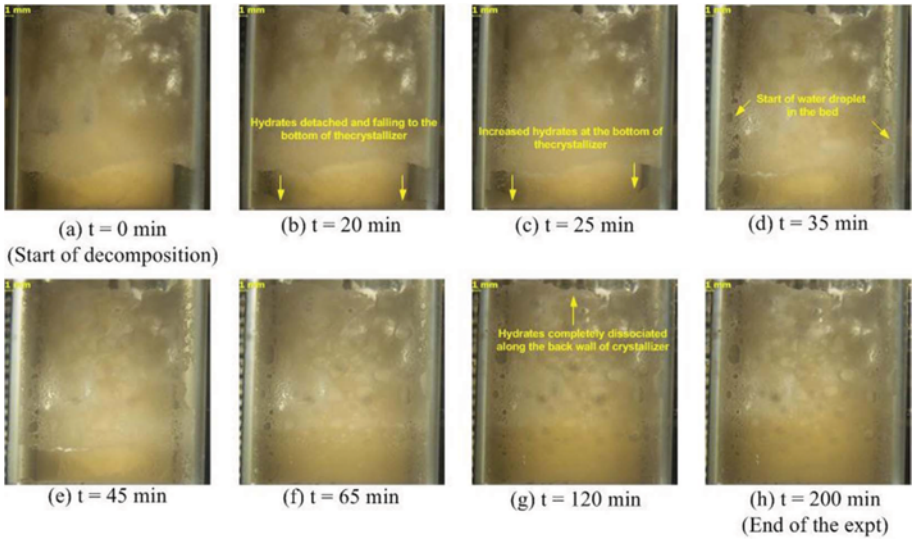


Fig. S7. Morphology of methane hydrates dissociation during the memory experiment in the hollow silica bed.

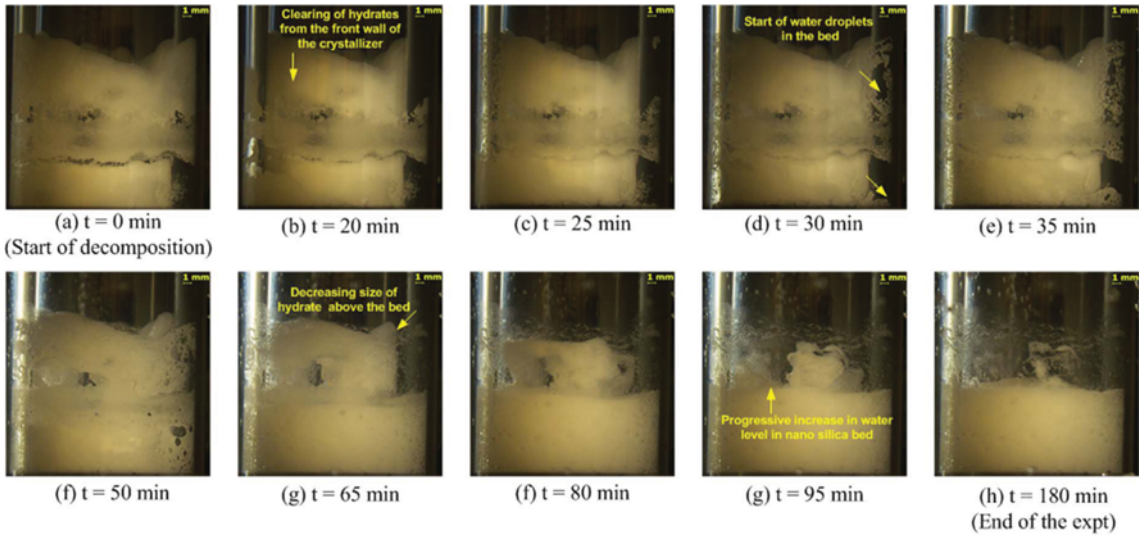


Fig. S8. Morphology of methane hydrates dissociation during the experiment without thermocouple in the hollow silica bed.

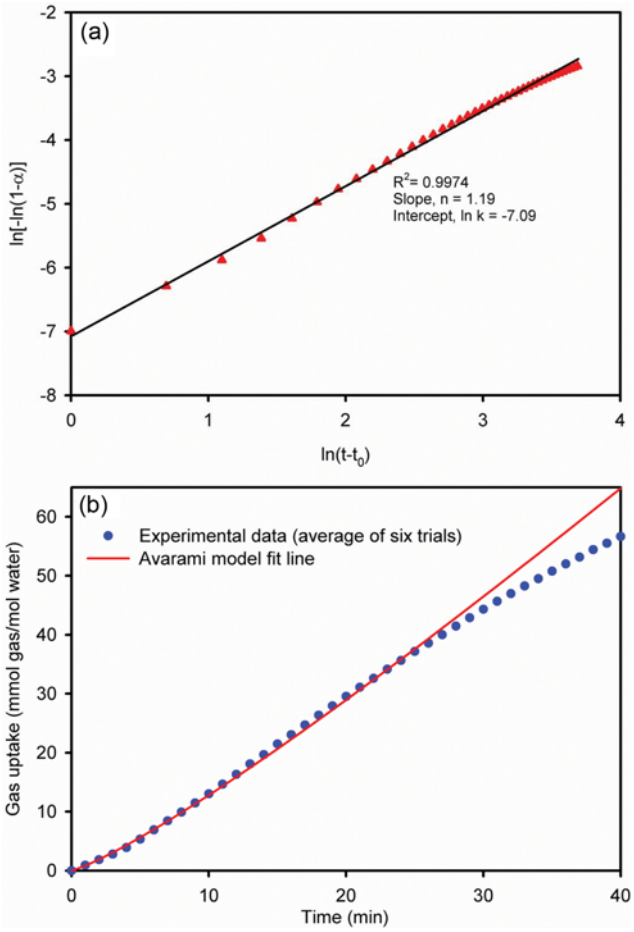


Fig. S9. (a) Plot of ln[−ln(1−α)] vs t for the determination of Avrami model parameters 'n' and 'k'. (B) Experimental and Avrami model fit for methane gas uptake for the first 40 min from nucleation.

REFERENCES

1. M. Avrami, *J. Chem. Phys.*, **7**, 1103 (1939).
2. M. Avrami, *J. Chem. Phys.*, **8**, 212 (1940).
3. M. Avrami, *J. Chem. Phys.*, **9**, 177 (1941).
4. R. Susilo, J. A. Ripmeester and P. Englezos, *AIChE J.*, **53**, 2451 (2007).
5. A. Nambiar, P. Babu and P. Linga, *Can. J. Chem.*, **93**(8), 808 (2015).